Chemical Engineering Journal 162 (2010) 278–295

Contents lists available at ScienceDirect

Chemical Engineering Journal

journal homepage: www.elsevier.com/locate/cej

No-moving-part valve for automatic flow switching

Václav Tesař*

Department of Thermodynamics, Institute of Thermomechanics v.v.i., Academy of Sciences of the Czech Republic, Dolejskova 5, 182 00 Prague, Czech Republic

ARTICLE INFO

Article history:
Received 4 November 2009
Received in revised form 13 April 2010
Accepted 15 April 2010

Keywords:
Fluid flow
Automatic control
Control valve
Fluidics

ABSTRACT

Flow control valve containing no moving components was developed for switching fluid flow passing through it into a parallel secondary path once the conditions in the main path reach a certain limit. No sensors or actuators are involved; the switching is caused by the inability of the Coanda effect to keep the flow attached to a wall that leads it into a particular outlet once a large resistance is met in this outlet. So far, there has been no method for designing such valves. To provide a guidance, this paper summarises experimental evidence about loading characteristics obtained with a considerable number of tested valve geometries.

1. Introduction

A requirement encountered quite often in systems with flowing fluids is quick switching of the flow in response to some change of the downstream state of the system. Common electronic control with actuated valves as a rule is not as quick as the flow system. Especially in critical situations, the quick action is demanded combined with the valve being fail-safe.

Solution to this difficult problem was found by author in fluidic flow control valves operating without moving parts. They are very reliable and need no maintenance. Also, they may be easily built as extremely robust and resistant to adverse conditions. It is possible to manufacture them from refractory or other difficult-to-machine materials and if the material is chosen properly, the valves can operate at extreme temperature, vibration, or nuclear radiation levels. The switching dependent on the downstream conditions is obtained in an interesting – and yet little known – category of fluidic valves. This is a segment of a more general class of fluidic devices that perform automatically certain control tasks without using any of the traditional control circuits approach: there are no sensors, no actuators and similar control-loop components, in traditional approach seemingly inevitable. Typically operation of these passive control valves is based on their special shape of loading characteristic. This is e.g. the case of the pressure regulator valve described in [1]. Another example is the fluidic valve in Rolls-Royce aero engine limiting the efflux of compressed air through a failed pipe [2]. Yet another valve was described in [3] to work with fluid as extremely difficult to handle as are molten metals. Of course, the operation without an external control signal, using just the hydrodynamics of a particular internal geometry, makes such valves exceptionally resistant and suitable for the most severe operating conditions – e.g., for handling chemically aggressive liquids – a requirement often encountered in chemical engineering.

The particular valve discussed in this paper was developed by the author to operate at high temperature levels – in fact glowing bright red. Its role, as shown in Fig. 1, is to protect the first-stage catalytic reactor (designed to operate instantly but only below certain temperature levels) by switching the flow of processed hot gas into a by-pass and this way into the second-stage reactor. The catalyst in the first stage has a relatively narrow window of temperatures in which it can operate efficiently. In particular, it is absolutely necessary to operate it so as to avoid the upper end of the window, beyond which the catalyst is in danger of irrecoverable changes. If the first stage is by-passed, the processing of the gas is done in the downstream second-stage reactor, with higher light-off temperature level and therefore unable to perform properly in those regimes where the first stage is active.

The valve performing this flow-diverting operation is extremely simple. In principle, it consists of only two plain components: a nozzle forming a jet and an attachment wall to which the jet adheres due to the Coanda effect. The latter is sensitive to the loading of the valve output and ceases to keep the jet attached at a certain level of the hydraulic resistance met in the connected device(s).

In the typical example of an application presented in Fig. 1, the system was designed to operate starting from lower supplied gas temperature, gradually increased and rising also due to the heat generated in the reactor due to the exothermic character of the reaction. At the lower temperatures, the jet issuing from the nozzle is guided into the first-stage reactor. As the gas temperature increases, so does its viscosity and this leads to increased hydraulic resistance opposing the flow in the small cross-section passages on the surfaces of which is immobilised the catalyst. The resistance

* Tel.: +420 2 6605 2270.
E-mail address: tesar@it.cas.cz.

1385-8947/$ – see front matter © 2010 Elsevier B.V. All rights reserved.
doi:10.1016/j.cej.2010.04.028

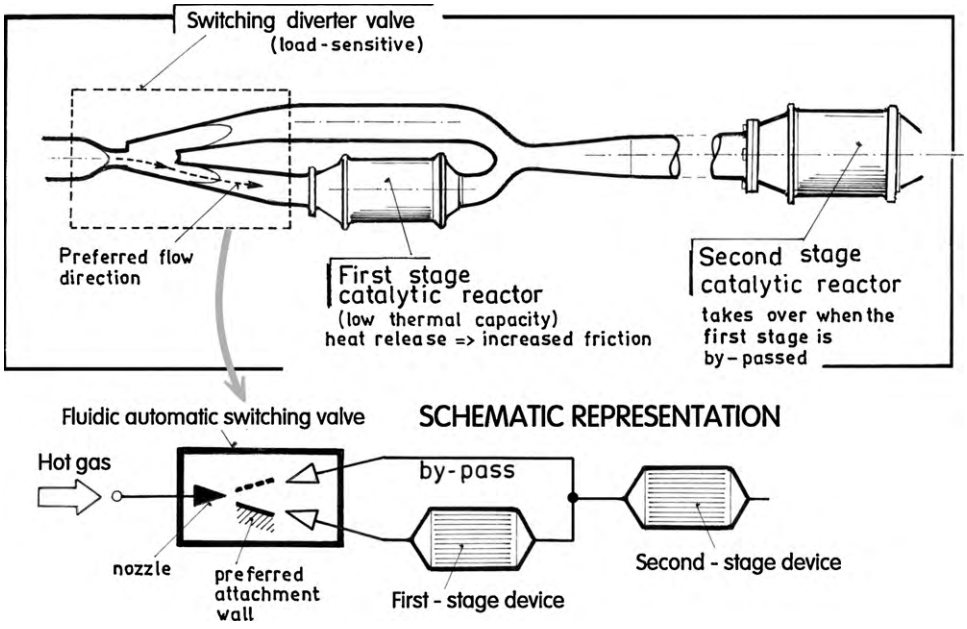

Fig. 1. The discussed diverter valve was developed for switching hot gas flow into the by-pass as soon as its increasing temperature – augmented by exothermic character of the reaction in the first-stage reactor – reaches the level at which the catalyst is in danger of an irreversible change.

makes the action of the Coanda attachment more difficult as it is much easier for the jet to leave the valve through the by-pass, where it does not meet such opposition. The essential problem for designing this fluidic circuit is adjustment of properties of the valve so that the loading at its output puts the critical measure of strain on the Coanda effect at exactly the right temperature [4].

This may seem to be a rather exceptional case of operating conditions – but, in fact, a similar need for the automatic switching action at a certain level of gradually increased loading is actually encountered quite often, as is documented by the second example presented in Fig. 2. This is a filtering system – operating at essentially constant temperature. The problem which the valve solves is the (usual) clogging of the filter by the particles (such as, e.g., dust) removed from the fluid. This increases the hydraulic resistance the flow meets. When the Coanda effect finally fails in its directing the flow into the main (primary) filter, the fluid flow is switched into the clean back-up filter – again automatically, without any external monitoring sensors and actuators.

The need to accelerate the fluid flow in the nozzle to generate strong enough Coanda effect may lead to high energetic loss in the valve (the loss being typically proportional to the square of flow velocity) and it is generally advisable to provide inside the valve some means for converting the fluid kinetic energy back into at least a part of the pressure energy the fluid had before entering the nozzle. This is the reason why there are in the valve the diffusers; their requirement of small divergence angle makes them quite long and at first glance the prominent parts of the valve. Apart from the main, preferential attachment wall there may be another wall on the other side of the jet path, guiding the flow into the vent terminal after the flow is switched.

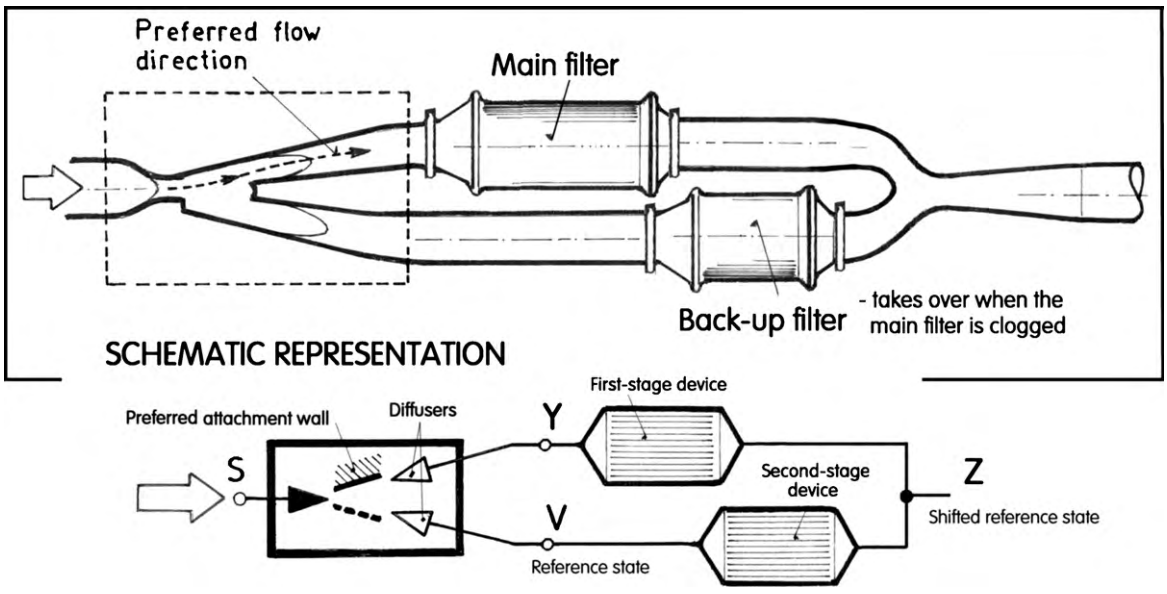

Fig. 2. Another example of the use of the automatically switching diverter valve, here removing the danger of the flow decreasing below an acceptable minimum due to the clogging of the main filter. With the back-up (the second stage) filter in place of the empty by-pass of the previous case (Fig. 1), the circuit design is slightly more complicated.

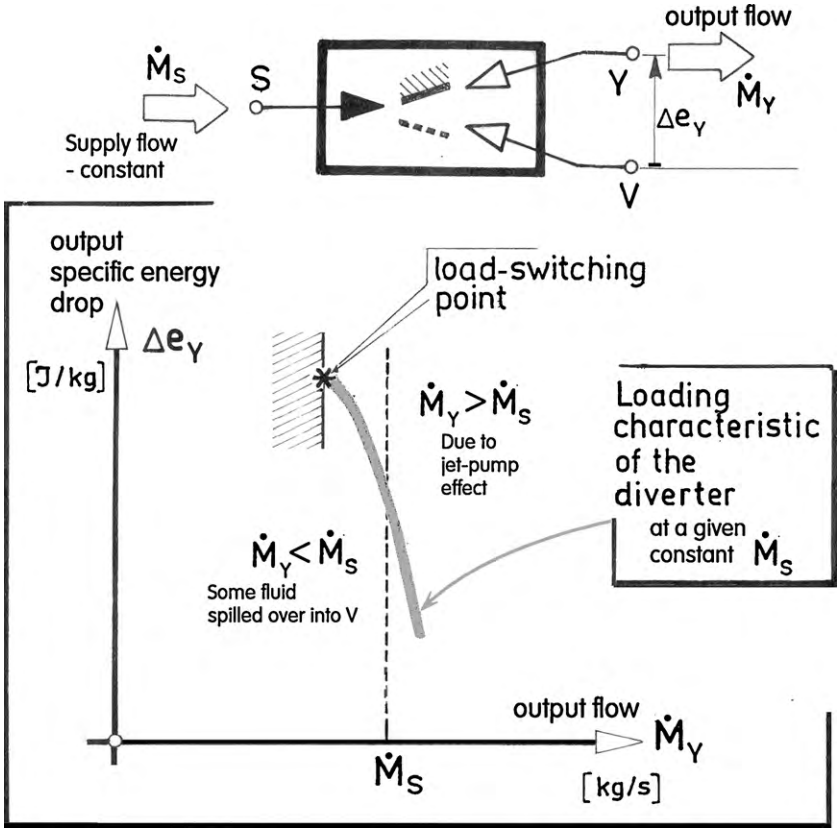

Fig. 3. The loading characteristic represents the decrease of the available output specific energy with increasing output flow rate. From the point of view of the subject of this paper, most interesting is the load-switching end of the characteristic.

The valves with automatic diverter switching in dependence on the loading are no new invention; they have been known and used – though only very sporadically – for more than two decades. Apart from the fact that the idea is little known, the reason for their rare use – much less than their undeniable advantages would suggest – is the lack of a design method sufficiently simple or at least straightforward. The loading properties upon which their operation is based, and the dependence of these properties on the geometry of the internal space (with its innumerable choices of various dimensions) are far from being understood. In all applications so far, the particular design has been a result of painstaking cut-and-try process. This paper aims at elucidating at least some of the rela-

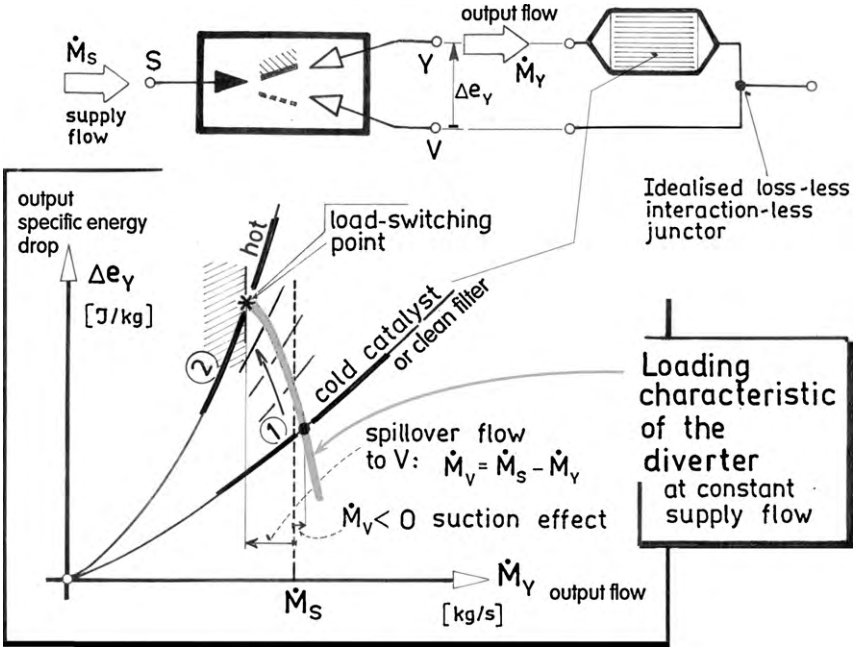

Fig. 4. The changes in the circuit from Fig. 1, evaluated graphically as the successive positions of the intersection of the valve loading curve (Fig. 3) with the characteristic of the load, gradually varying from (1) to (2).

tions between some of the design parameters in the resultant valve behaviour.

2. Loading characteristic of the valve

In contrast to mechanical flow diverting valves with moving parts, in which the fluid is prevented from entering a particular flow path under any conditions – by blocking materially the entrance into it – operation of fluidic flow control diverter valves without moving parts depends on more subtle balance. Proper conditions in the fluidic circuit have to be carefully set up, taking into the consideration the properties of the valve as well as those of the device connected as the load to its output terminal. The adjustments are best made by following the mental guidance of a graphical representation. One of the reasons why this is so useful is the usual fact of the properties of fluidic devices being typically strongly non-linear and therefore not easily expressed by a simple formula.

For the purposes of the circuit design the valve properties are most usefully described by graphical presentation of the loading characteristics – a dependence of the output specific-energy difference on the output flow rate – a generic example of which is presented in Fig. 3. In contrast to a mechanical valve, typically delivering to its output terminal exactly all the fluid flow supplied into the inlet, the jet-type fluidic valve properties are not so simple. Their output flow rate in the output terminal Y may be higher than the supplied flow rate into S since the jet generates the jet-pumping effect, entraining additional fluid through the vent terminal V. On the other hand, throttling the output flow – which may be done in an attempt to obtain higher specific energy in Y (and therefore higher available acting pressure, since the pressure energy component usually represents most of the available energy of the fluid) – causes spilling of some supplied fluid over into V. The end of the characteristic curve approached by the throttling is of particular importance for the subject of this paper: it represents the state in which the gradually increased throttling (by decreasing available cross-section in the connected load) overcomes the capability of the Coanda effect to keep the flow attached to preferred attachment wall and all the flow is switched into the vent V.

Fig. 4 presents graphically the conditions in the circuit from Fig. 1 (the case with empty by-pass; for simplicity of the presentation the hydraulic loss in the by-pass pipe is here neglected). In this case the output specific energetic difference between the valve terminals Y and V is equal to the specific-energy drop Δe across the load. This is dependent on the flow rate passing through the load; the dependence is the *characteristic* of the load. In fluidics in general, especially at high Reynolds numbers, the characteristics are usually more or less quadratic, capable of being fully described by the value of the quadratic dissipance Q:

$$\Delta e = Q\dot{M}^2. \tag{1}$$

In the present case the characteristics of the load devices – those which are strongly influenced by viscosity changes in long narrow channels – tend to require also a considerable linear term [5,8]. The coefficient in this term may be expressed as a multiple of Q:

$$\Delta e = Q\dot{M}^2 + rQ\dot{M}. \tag{2}$$

The gradually increasing Δe at the same flow rate due to clogging or viscosity increase is represented in Fig. 4 by the succession of the device characteristics progressing from (1) to (2) (those between these extreme cases are shown only in part). The states in the circuit are determined by the intersections with the characteristic of the valve. In the initial cold-start state (small resistance) there is in the case represented in Fig. 4 a small negative flow (i.e. directed backwards into the valve) in the vent terminal V (through the by-pass). This means the flow passing through the loading device is larger than the flow rate supplied into the nozzle. This effect may be avoided by a different choice of properties of the devices. Alternatively, this re-circulation of the fluid in the valve exit loop may be useful: e.g., in the case of a filter this ensures removal of any particles that manage to get through during the first pass – and in the case of a catalytic reaction the re-circulation increases the yield. Gradually, the conditions usually change into the regime of considerable spillover into the vent and finally approach the load-switching state.

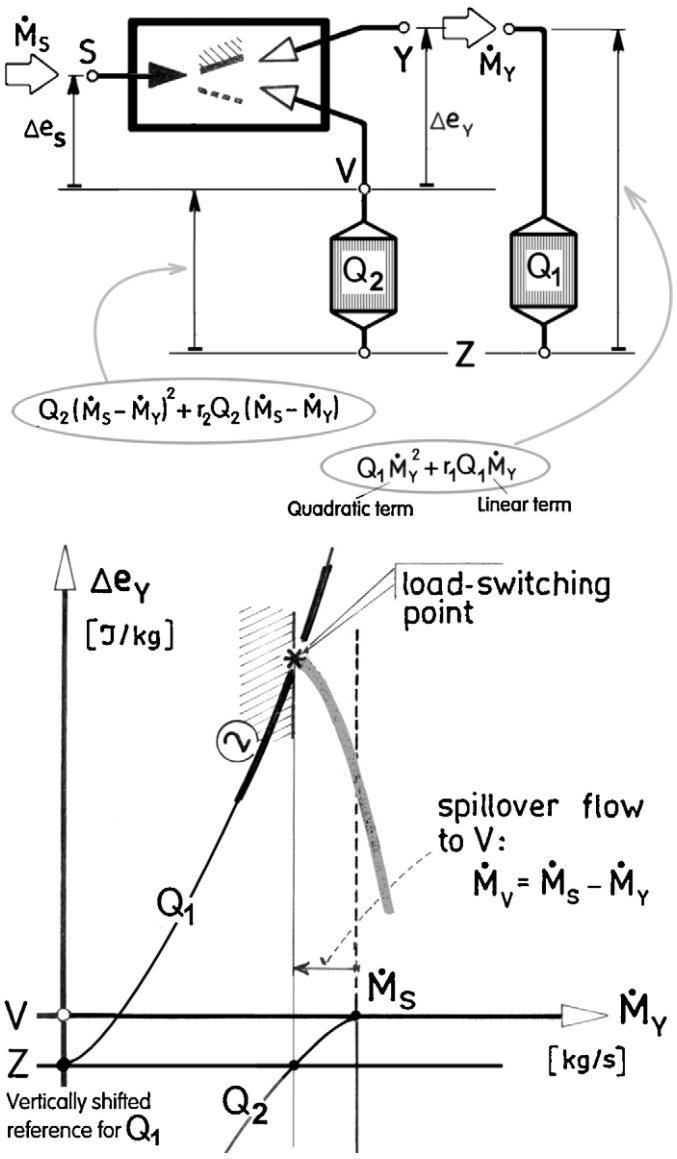

Fig. 5. In the case of Fig. 2 the load-switching conditions are evaluated from the intersection of the valve loading curve with the characteristic of the load in its hot (or clogged) high resistance state (2) shifted down by an amount representing the specific-energy drop across the second-stage device Q_2.

The characteristic of the valve (as presented in Fig. 3) is, of course, useful also in the case with a loading device placed into each of the two outlet flowpaths, according to Fig. 2. The graphical presentation used to evaluate the load-switching conditions for this case is shown in Fig. 5. The characteristic of the main, first-stage device positioned in the preferred exit Y is shifted down by the distance evaluated according to Eq. (2) for the parameters Q_2 and r_2 of the second-stage device as well as for the spillover flow $\dot{M}_S - \dot{M}_Y$.

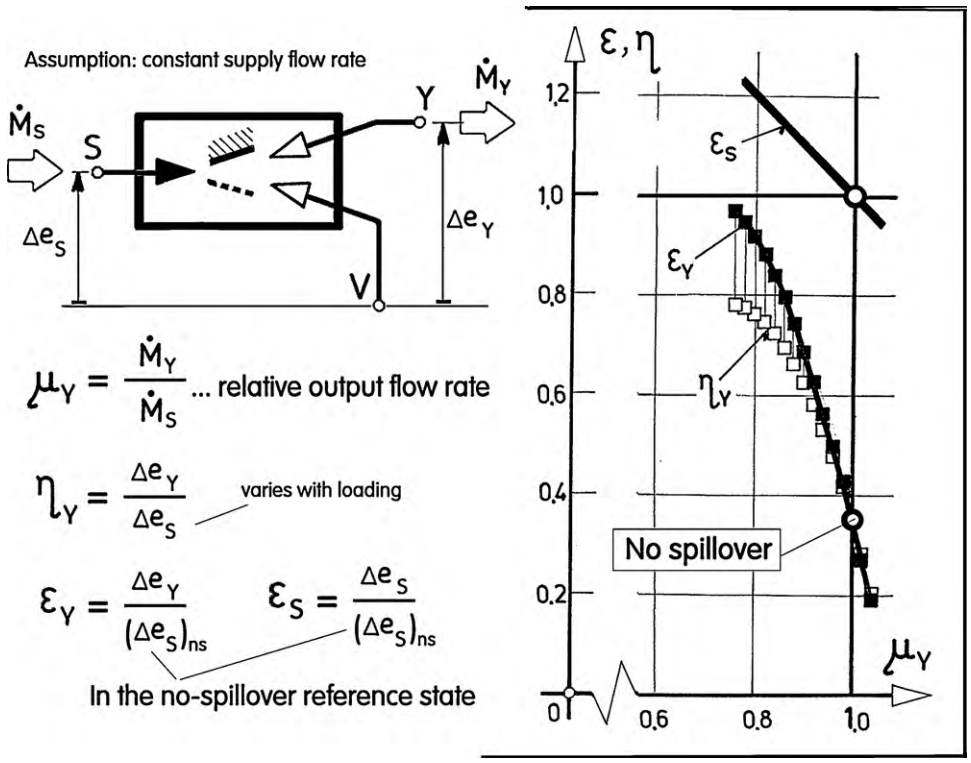

Fig. 6. Transformed dimensionless co-ordinates bring the advantage of universality – apart from small dependence on Reynolds number, the loading characteristic is practically the same for any magnitude of the supply flow rate.

Calculations follow the graphical representations – in the cases discussed above they are performed with absolute values of the flow rate and fluid specific energy. For general description of the valve loading properties it is useful to transform the loading characteristic into the dimensionless co-ordinates as they are presented in Fig. 6. Because of the Eulerian similarity [10], the whole family (theoretically consisting of infinitely many members) squeezes into a single universal curve [11] – perhaps with some small non-coincidences due to Reynolds-number dependence. The output flow rate is non-dimensionalised by relating it to the supply flow rate

$$\mu_Y = \frac{\dot{M}_Y}{\dot{M}_S} \tag{3}$$

and, in a similar manner, the output specific-energy difference is non-dimensionalised by being related to the supply specific-energy difference Δe_S (between the supply terminal S and the reference V)

$$\eta_Y = \frac{\Delta e_Y}{\Delta e_S}. \tag{4}$$

A fact not universally recognised is internal flowfield in the valve changing with the loading. This means also the supply specific-energy difference (Fig. 5) Δe_S varies as the relative flow rate μ_Y is changed. As a result, the shape of the resultant dimensionless loading curve

$$\eta_Y = f(\mu_Y) \tag{5}$$

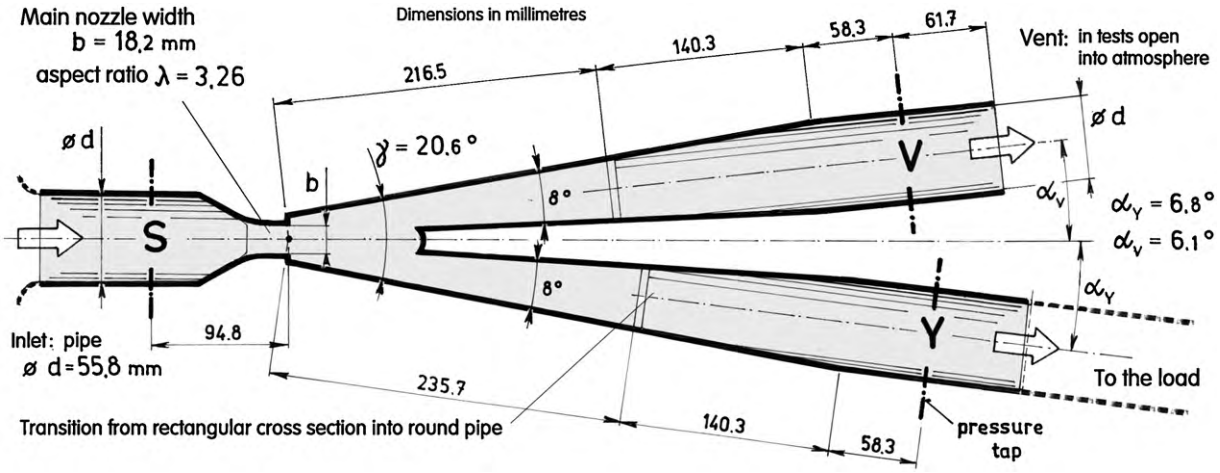

Fig. 7. Overall geometry and dimensions of the full-scale laboratory test model, with round-pipe inlet as well as outlets while the central core part (of critical influence on the properties because the velocities there were high and aerodynamic effects most pronounced) was of rectangular, constant-depth cross sections.

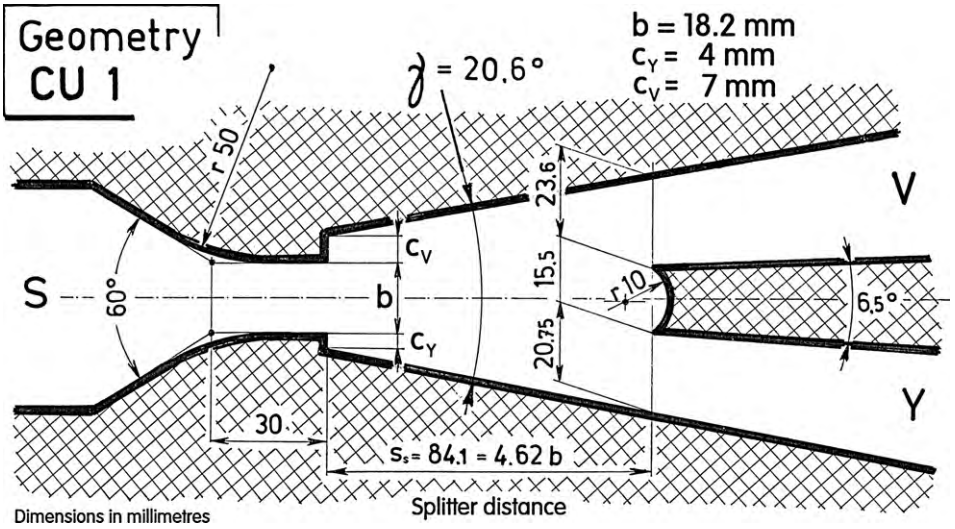

Fig. 8. Geometry of the valve core in the first of the tested variants. The depth – perpendicular to the drawing plane – was h = 52.8 mm, the same everywhere throughout this core.

differs from the shapes of the original loading curves in absolute co-ordinates

$$\Delta e_Y = f(\dot{M}_Y). \tag{6}$$

This was first noted by Tippetts and Royle [9] (actually for the related bistable amplifiers), who recommended avoiding this by taking as the reference not the supply specific-energy difference in the particular evaluated state but, instead, the supply specific energy $(\Delta e_S)_{ns}$ in the no-spillover regime, i.e. at the relative output flow $\mu_Y = 1$. This means evaluating a different dimensionless output specific energy:

$$\varepsilon_Y = \frac{\Delta e_Y}{(\Delta e_S)_{ns}}. \tag{7}$$

Also, it should be noted that it is possible (and useful) to evaluate the analogous expression for the variations of the relative difference between the supply terminal S and V

$$\varepsilon_S = \frac{\Delta e_S}{(\Delta e_S)_{ns}} \tag{8}$$

the dependence of which on the relative flow rate

$$\varepsilon_S = f(\mu_Y) \tag{9}$$

should be also investigated and plotted in the full dimensionless output characteristic diagram.

The example at the right-hand side of Fig. 6 shows the difference in the curve shapes in the two dimensionless presentations by Eq. (5) and by

$$\varepsilon_Y = f(\mu_Y) \tag{10}$$

for a simple linear variations of Δe_S with the loading. In the following discussion of experimental results obtained with different tested valve variants, the attention is focused on the shape-retaining non-dimensionalisation with respect to $(\Delta e_S)_{ns}$, i.e. using Eqs. (9) and (10). Because of the Eulerian similarity being not perfect, each such data set should be accompanied by a statement about the value of the test Reynolds number, usually evaluated for the conditions in the exit of the nozzle.

3. Tested model valve

The valve used in the laboratory investigations was derived from a design intended for operation at a rather large scale, processing exhaust gas flow [7] in a system of devices [5] connected by 2.5 in. outer diameter pipes. This size was retained in the model, but the tests did not simulate the exhaust gas system conditions and were performed with steady, non-pulsating cold air flow. It should be noted that pulsations, such as those encountered in an internal combustion engine exhaust [7], would actually considerably change the results, since even at large divergence angles of the attachment walls the pulsating flow would tend to attach to both of them – a strongly pulsating flow would certainly not produce the desirable Coanda effect in the 20.6° wall divergence cavity of the present model shown in Fig. 7.

The valve geometry was complicated by the transitions between the circular cross-sections in the terminals and the constant-depth geometry, i.e. rectangular cross-sections in the core part (Fig. 8). Due to the constant depth in this part, the geometry there is essentially two-dimensional. This, however, cannot be said about the internal flowfield there. The small, 20.6° total divergence was chosen in an attempt to minimise the hydraulic losses associated with change of flow direction.

To secure the property of the flow in unloaded valve always passing into the output terminal Y, the design as seen in Figs. 7 and 8 is visibly asymmetric. The inclination of the attachment wall is smaller on the Y side $\alpha_Y < \alpha_V$ (Fig. 7). Also there is a larger setback $c_Y < c_V$ (Fig. 8) on the vent side. The jet in the starting flow regime always attaches to the wall with smaller setback and smaller inclination angle – and this ensures that fluid is directed into the output terminal Y. Apart from this Coanda effect preference, in the basic

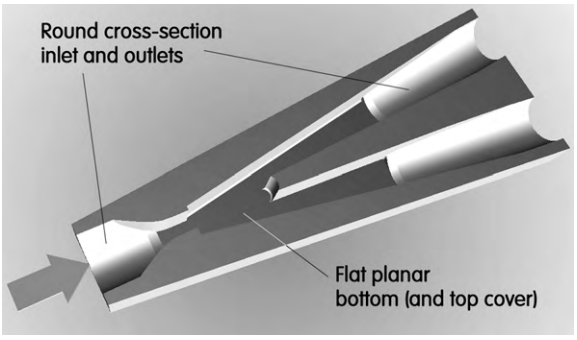

Fig. 9. The lower half of the computational domain used in the numerical flowfield computations. The picture presents instructively the transitions between the round cross-sections of the inlet and outlet pipes and the rectangular (constant-depth) cross-section shape of the core.

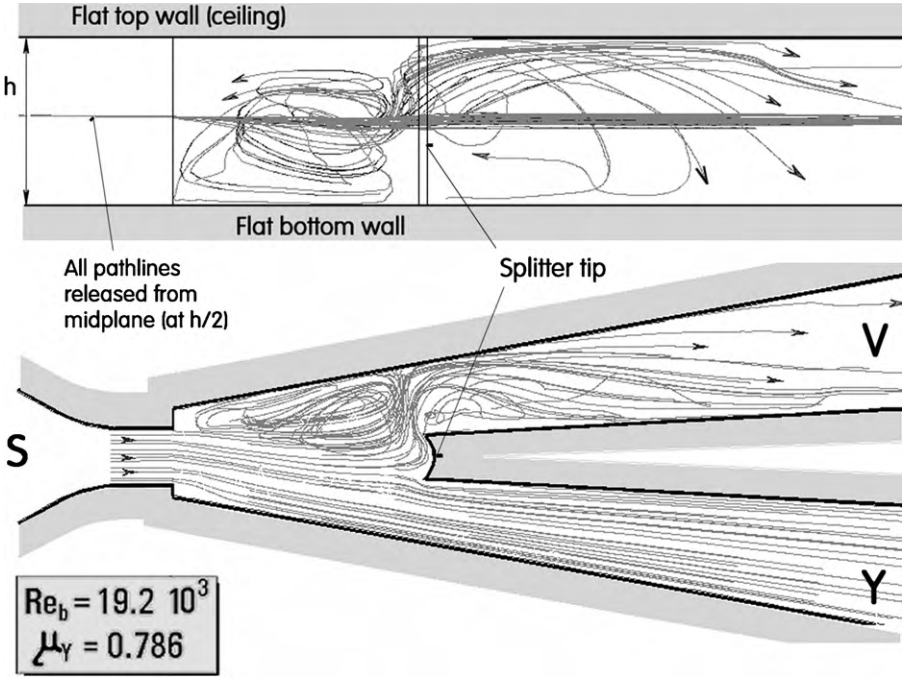

Fig. 10. An example of computed pathlines obtained for rather typical conditions demonstrates the unexpected strong three-dimensionality of the flowfield. The pathlines (trajectories of imagined particles left to follow the local flow directions) were all released from the same midplane height and yet some of them soon reached as low as to the bottom and others as high as the top cover plate.

design shown in Figs. 7 and 8 stabilisation of the deflected jet flow into Y, was augmented by providing the internal positive feedback loop – by the bi-cuspid nose of the splitter with the concave wall between the cusps, in a similar manner as was found useful earlier (e.g. in [12,13]).

Present paper is devoted exclusively to the results obtained by experimental investigations. In fact they were supported by independent numerical flowfield computations, performed using the standard FLUENT software in the fully three-dimensional computational domain, the bottom half of which is shown in Fig. 9. The fully 3D solutions were chosen because of the expected complications associated with the circular/rectangular/circular transitions in the flowpath cross-sections. Considering the essentially two-dimensional geometry of the critical part of the valve as shown in Fig. 8 (and also considering the relatively large aspect ratio, making less influential the effects of the friction on the top and bottom flat walls there), no significant three-dimensionality of the flowfield in the valve core was initially expected. The more surprising was therefore the fact of there being actually a very strong three-dimensionality, as documented in Fig. 10. Obviously, the computations have shown the pathlines in the collector leading to the vent V to be actually helical in shape. This explains the common failures of some fluidic device designers who attempt evaluation of the internal conditions by simple one-dimensional calculations

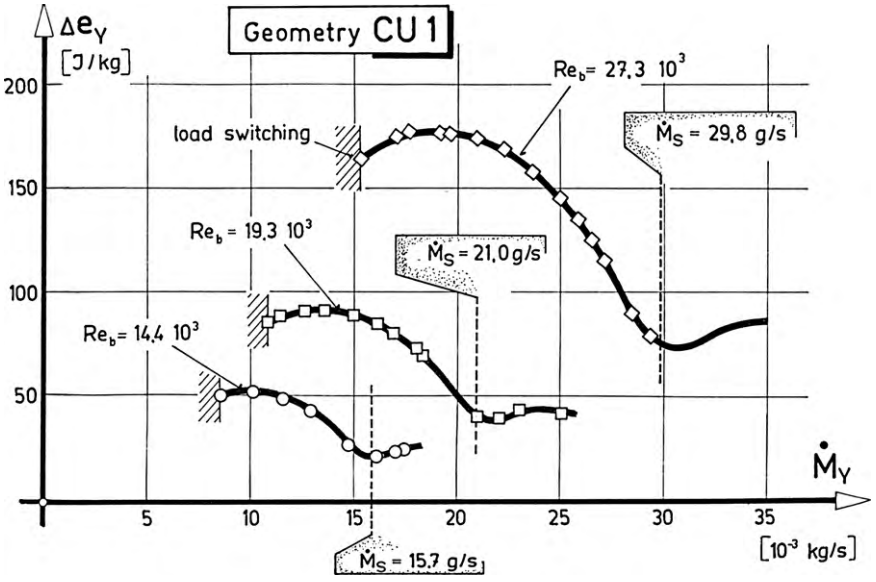

Fig. 11. The loading characteristics in absolute co-ordinates according to Eq. (6) obtained in the experiments with the baseline model (Figs. 7 and 8). Three independent measurement runs were made, each at different constant supply mass flow rate (note the corresponding values of Reynolds number, computed from the nozzle exit width).

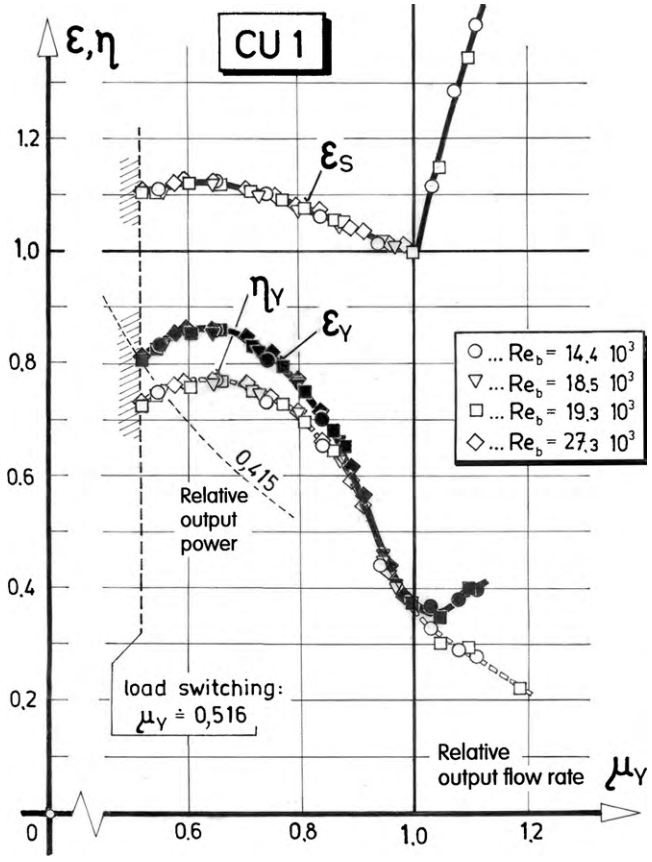

Fig. 12. Demonstration of the validity of the Eulerian similarity: all experimental data obtained for the baseline valve (Figs. 7 and 8) fall on the same curves in the dimensionless co-ordinates Fig. 6.

based only on the size of the cross-sectional areas. In particular, the behaviour of the diffusers may be in some regimes significantly influenced by the complex character of the flowfield at their entrances. The helical character of the flow inside the valve is an important feature that underlines the general importance of helical flow mode instabilities in fluid mechanics, as discussed, e.g., in [16,17].

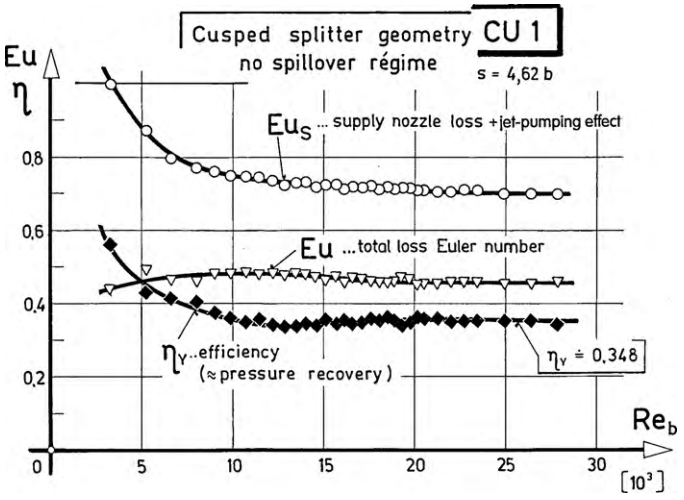

Fig. 13. Experimental dependence of the loss coefficient (Euler numbers) and valve efficiency of the baseline CU1 model on Reynolds number.

4. Experimental results with the baseline geometry

The experiments with the valve in its initial geometry, as shown in Figs. 7–9, were run on four occasions, at four different constant air mass flow rates supplied into the nozzle. The flow rates into the output Y were gradually more and more restricted and – together with the supply flow rate, measured and kept constant – were measured by an orifice flowmeter. The pressure differences measured between the locations S, Y, and V (the positions of these locations are indicated in Fig. 7) were converted into the differences in specific pressure energy, to which were added the local values of the air specific kinetic energy computed for the same locations. Because of the relatively large cross-sections there, the pressure component was dominant in Δe_Y.

The values Δe_Y for the three test runs are plotted in Fig. 11 as a function of the mass flow rates. All three curves are mutually similar. In the following Fig. 12, the collected experimental data (including those from Fig. 11) are plotted converted into the dimensionless values using the expressions listed in Fig. 6. Indeed, due to the similarity, all the data in the transformed co-ordinates $\varepsilon_S = f(\mu_Y)$ fall on a single curve. Also plotted is the supply charac-

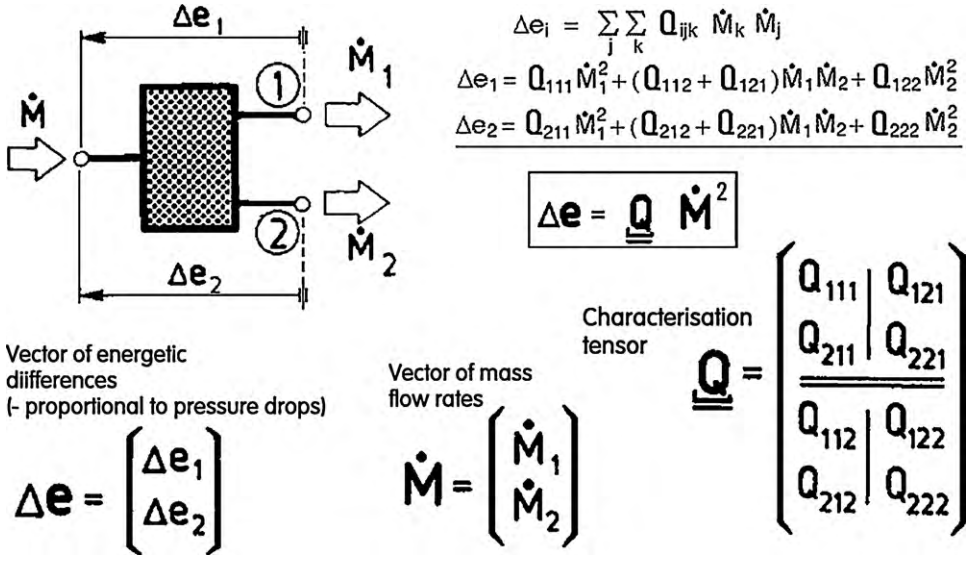

Fig. 14. A general concept of bifurcator element (with one inlet terminal and two outlets) [18]. Its dependence of the vector of energetic drops on the vector of mass flow rates is defined by the third-order multiplication tensor of general quadratic dependence between two vectors.

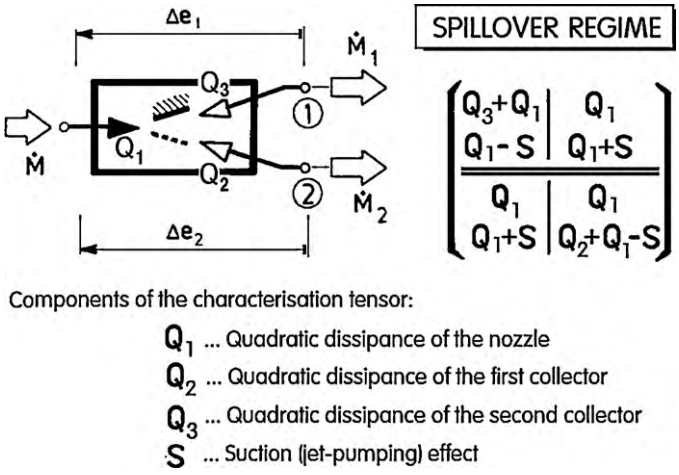

Fig. 15. The valve in the spillover regime is a case of the bifurcator (Fig. 14). The components of the characterisation vector in this case posses a simple physical meaning.

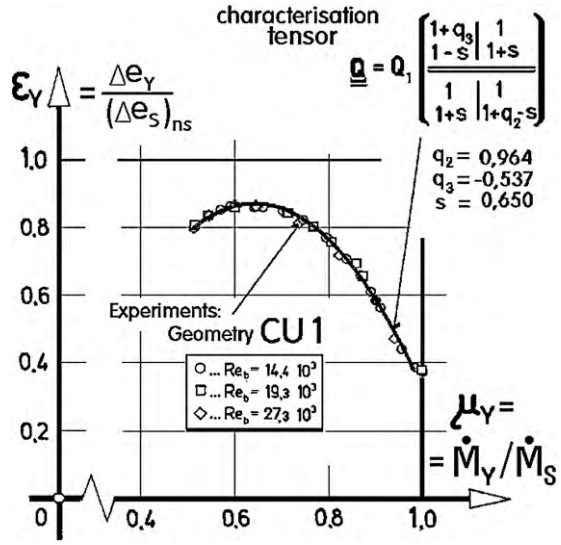

Fig. 16. It is possible to identify the values in the third-order characterisation tensor of Fig. 15 the insertion of which into the general quadratic vector-to-vector mapping function of Fig. 14 produces a loading characteristic exactly corresponding to the experimental findings.

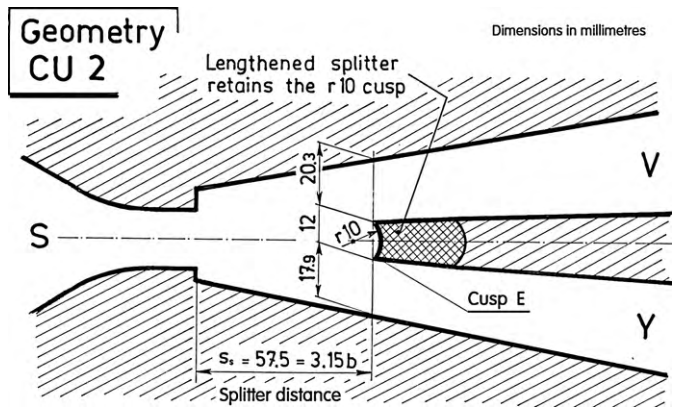

Fig. 17. Geometry of the baseline model adapted to very short distance s_s from the nozzle exit to the splitter nose. According to general belief, the shorter length of jet losing momentum by mixing with slower outer fluid should result in higher efficiency.

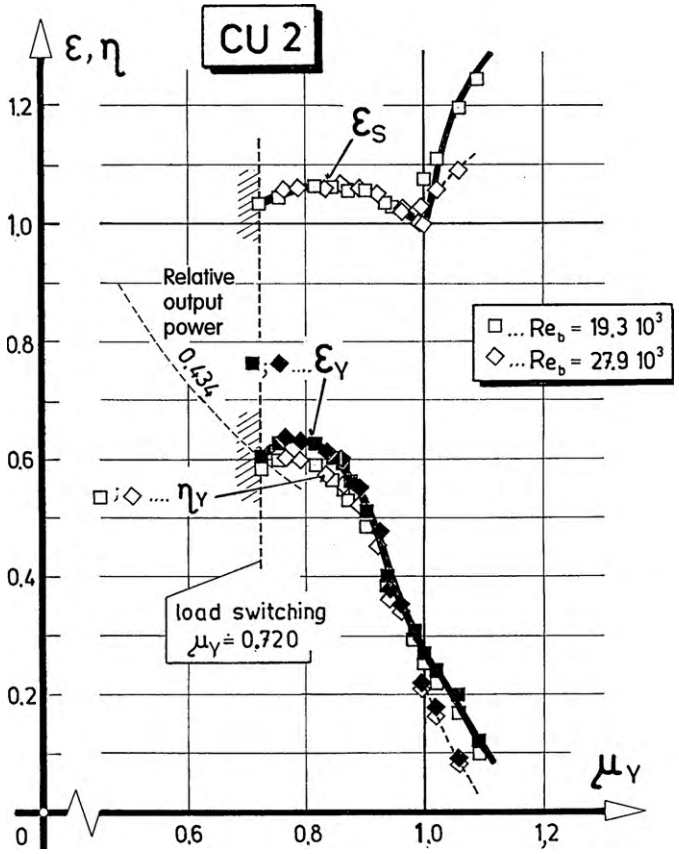

Fig. 18. Experimental complete output characteristic, in similarity co-ordinates, of the valve in the geometry variant CU2 as shown in Fig. 17.

teristic $\varepsilon_Y = f(\mu_Y)$ making the diagram Fig. 12 the complete output characteristic of the valve. A remarkable fact seen there is the substantial change in the character of the flowfield, markedly revealed by the sudden kink in the supply curve during transition, in the no-spillover state $\mu = 1$, from the regime with positive spillover into the jet-pumping regime. Also of interest in Fig. 12 is the position of the load-switching point and the hyperbolic line of constant relative output power, evaluated for the state just before switching.

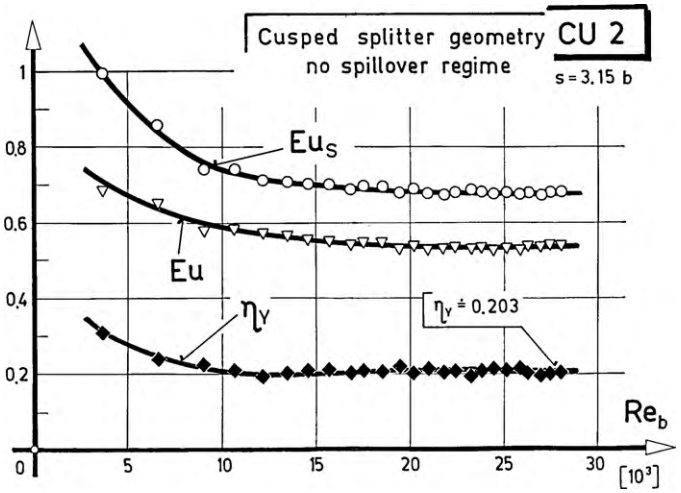

Fig. 19. Experimental Reynolds-number dependence of the loss coefficient (Euler numbers) and valve efficiency for the variant CU2 from Fig. 17. Comparison with Fig. 13 indicates a larger proportion of Reynolds-number dependent friction loss component and – contrary to expectation – lower efficiency.

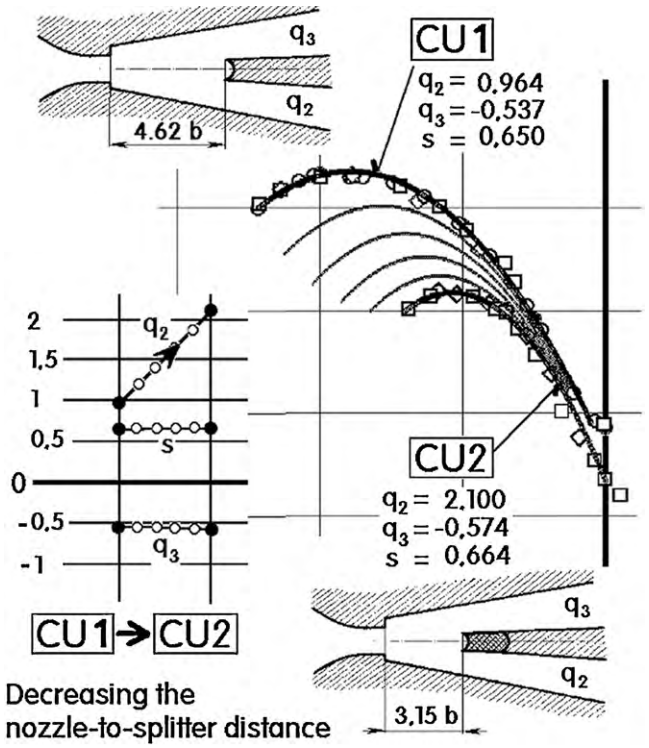

Fig. 20. Comparison of the loading curves for the two cusped-splitter geometries. Identified numerical values of the coefficients in the characterisation tensor of Fig. 15 show the lengthened splitter results just in increased dissipance of the first (preferred) collector – and the corresponding deterioration of valve properties.

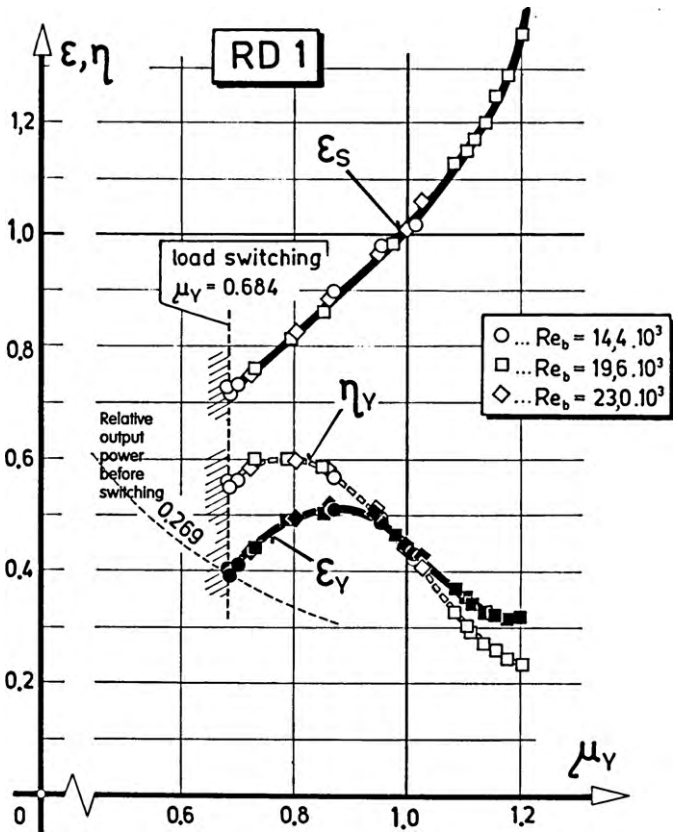

Fig. 22. Experimental complete output characteristic, in similarity co-ordinates, of the valve in the adapted version with rounded splitter geometry RD1.

Somewhat disappointing may be the relatively low efficiency of the valve – mere 37% in the no-spillover state. Obviously, because of the dominance of the pressure component in the specific-energy differences, this reflects a rather poor pressure recovery in the valve. This is rather surprising, considering the very short nozzle-to-splitter distance $s_s = 4.62b$ (Fig. 8) much shorter than the usual values in fluidic amplifiers with much longer distance s_s and therefore providing more opportunity for the jet to lose its momentum. The traditional line of thinking is the pressure recovery to be mainly a matter of the conversion that takes place in the diffuser(s) and here the jet is guided into them without being given much opportunity to lose its momentum by mixing with slow external air. Admittedly, their relatively large 8° divergence angle (Fig. 7) makes the diffusers in this model not the most efficient ones, but the value

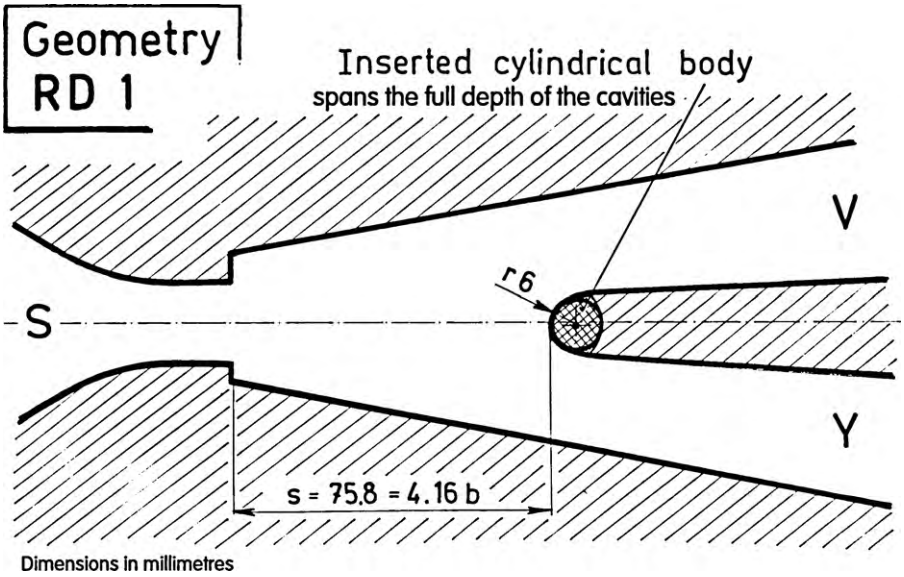

Fig. 21. Valve geometry adapted to convex splitter shape intended to answer repeated questioning of the wisdom of author's bi-cuspid splitter nose [12].

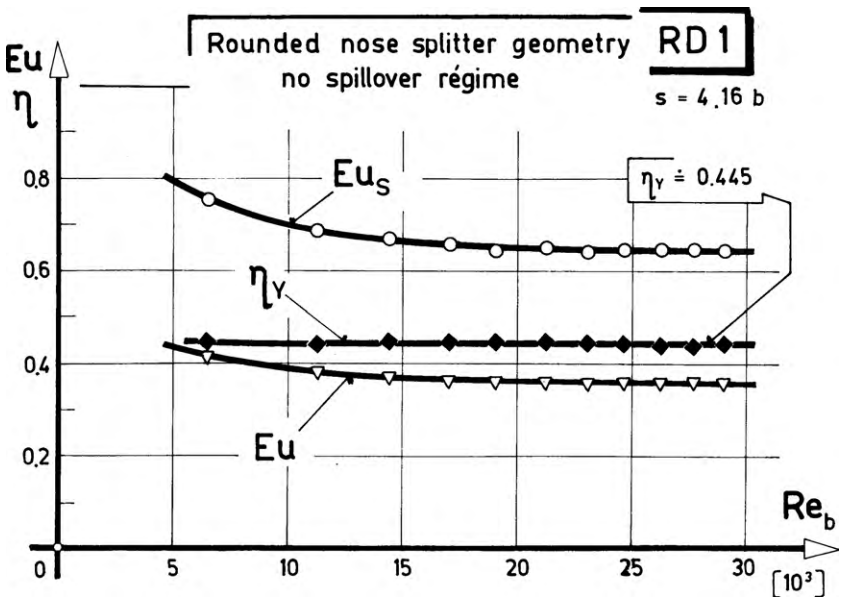

Fig. 23. Experimentally determined loss Euler numbers and efficiency for the valve variant shown in Fig. 21. In comparison with Fig. 13, the rounding of the splitter brings some improvement in efficiency which, however, loses its interesting trend of improving with decreased Reynolds number.

is not so large as to make the diffuser performance really poor. Recent discovery of the dominant role of a different pressure recovery mechanism [13] was, of course, not known at the time when the valve was designed. It is probable that it is an unfavourable condition for this trapped-vortex mechanism that was the real reason for the disappointment.

Obvious pre-requisite for the remarkably good similarity demonstrated in Fig. 12 is the small dependence of the character of the internal flowfield on Reynolds number. This dependence, experimentally found for the valve from Figs. 7 and 8, is presented in terms of Euler numbers and valve efficiency in Fig. 13 – as functions of Reynolds number evaluated from the nozzle exit conditions. The values plotted there were all obtained in the no-spillover regime. Indeed, most of the values there are very near to a constant, at least at the sufficiently high Reynolds numbers as were those indicated in Fig. 12 as the conditions of the experimental runs. Significant deviations from the quadratic similarity were found only at very low Reynolds numbers. Especially remarkable there is the increasing efficiency at low Re, a feature that may be of some significance for the low Reynolds numbers microfluidics (e.g., [14]).

5. Characterisation by the third-order tensor

The graphical representation of properties by the characteristic curves, as shown in Fig. 12, provides an instructive guidance for the circuit design, but is not suitable for working with it on a computer. For the purposes of storing the data and performing the design calculations it is preferable to have an analytical description of the device.

In electronic circuits, the properties of analogous three-terminal devices for such purpose are usually expressed by a matrix that defines a linear dependence between the vectors of currents and voltages. This is not applicable in the non-linear case of the fluidic valves. What may be taken over is only the essential idea of the characterisation by the dependence between the vector of mass flow rates and a corresponding vector of specific-energy drops (Fig. 14). Because of the usually dominantly quadratic character of the dependences in fluidics, the dependence is with sufficient accuracy expressed using the vector-to-vector quadratic dependence [15]

$$\Delta e_i = \sum_j \sum_k Q_{ijk} \dot{M}_k \dot{M}_j \tag{11}$$

as shown in Fig. 14. The third-order tensor that defines this dependence is the characterisation tensor Q_{ijk} containing the multiplicative coefficients. In fact, the individual terms of these

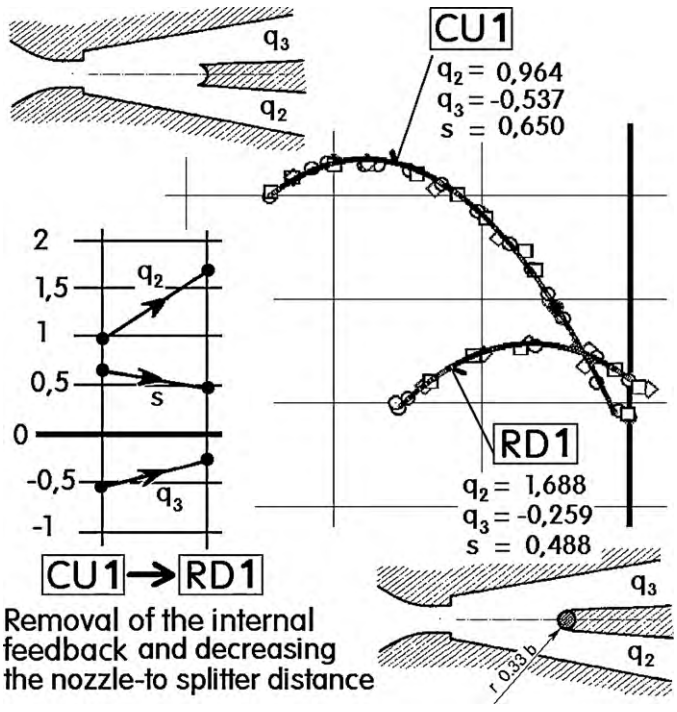

Fig. 24. Comparison of the loading curves for the baseline geometry CU1 and the adapted round-nosed RD1. The values in the characterisation tensor of Fig. 15, obtained by identification procedure, show the round splitter nose increases the collector losses (to a recognisable extent more in the preferred collector, leading to output terminal Y) and decreases the effectiveness of the interaction term s.

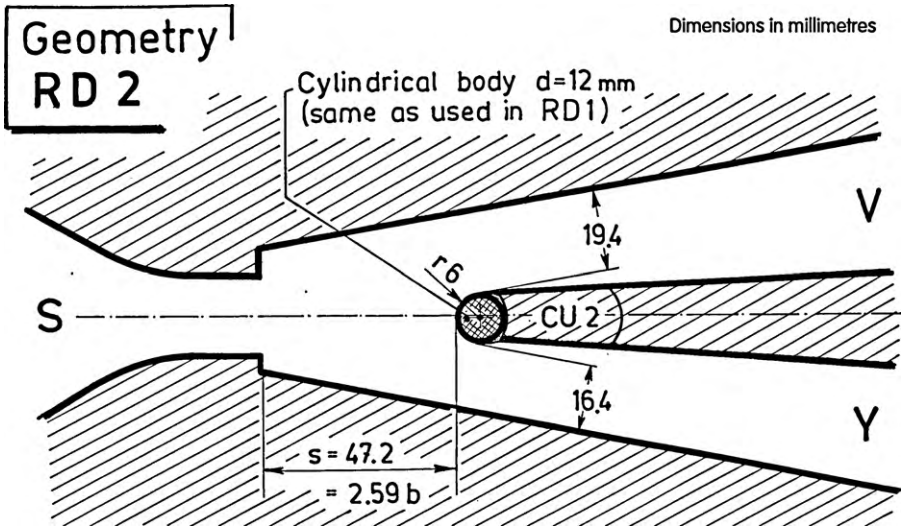

Fig. 25. Another investigated adaptation of valve geometry, with rounded splitter at a short distance from the nozzle exit.

coefficients may be easily demonstrated to posses reasonable physical meanings, a listed in Fig. 15. The terms Q_i characterise, similar as does the scalar value of quadratic dissipance Q in Eq. (1), the energetic losses in the individual parts (components) of which the valve consists: the nozzle and the two diffusers. Apart from the loss terms, there is also the suction term S. If it were absent, the tensor Q_{ijk} consisting of only the quadratic dissipances would be symmetric. It is the anti-symmetric part (the "suction" – actually here involving all the more complex effects of jet flow interactions) that makes this tensor approach suitable for the description of the valve as a bifurcator element. It is possible to extract the most important and easiest to evaluate dissipance – the value Q_1 for the nozzle – so that for the description of all characteristics in the relative co-ordinates it is necessary to evaluate just the three numerical values of the relative magnitudes of the terms:

$$q_2 = \frac{Q_2}{Q_1} \tag{12}$$

$$q_3 = \frac{Q_3}{Q_1} \tag{13}$$

and

$$s = \frac{S}{Q_1}. \tag{14}$$

Their magnitudes were identified for the valve in its baseline geometry CU1 and are presented in the upper-right corner of Fig. 16, the rest of this picture showing how successful is this description of the valve properties compared with the graphical presentation of the loading characteristic.

6. Changing the splitter distance

The jet leaving the nozzle in the valve loses its momentum – and specific kinetic energy – by mixing with the slower outer fluid in the interaction cavity. Compared to this, the loss due to its surface friction when it is attached to the inclined attachment wall, though considered by some inexperienced observers a source of hydraulic losses in the valve, is relatively insignificant. There is a general consensus that to keep the valve efficiency at a reasonable level, the jet flow has to be converted as soon as possible into the wall-bounded flow in the diffuser. For this, the valve geometry should be designed with as short as possible nozzle-to-splitter distance s_s. Some distance travelled by the jet, nevertheless, is necessary to provide it with an opportunity to the switching motions. In the successful bistable diverter valve reported in [12] the relative value of this distance was

$$\sigma = \frac{s_s}{b} = 6.85 \tag{15}$$

and this was considered exceptionally small value compared with other known Coanda effect valves. In Fig. 8, this relative value for

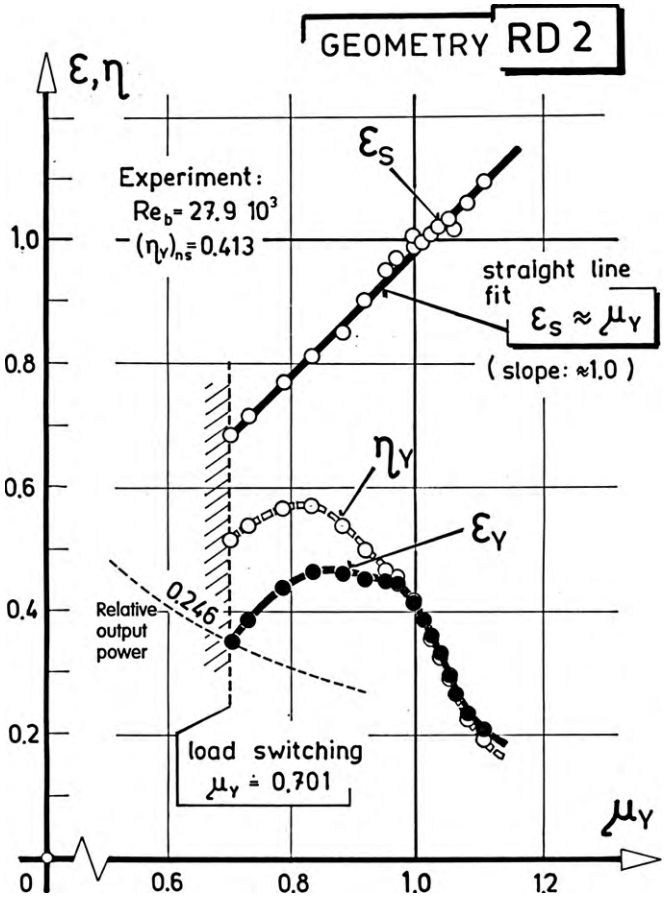

Fig. 26. Output characteristic, in similarity co-ordinates, of the valve in the version from Fig. 25. Comparison with Fig. 22 shows that even a substantial change in the nozzle-to-splitter distance with the round-nosed splitter surprisingly does not lead to a significant change of the loading curve in the spillover regime.

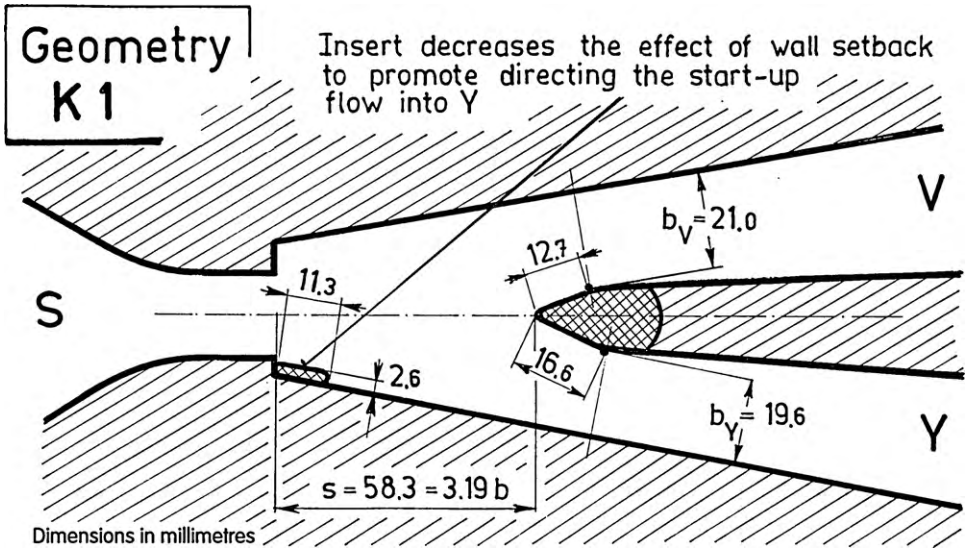

Fig. 27. Investigated valve variant with sharp wedge splitter shape. To ensure the preference of the output Y, the setback of the main attachment wall had to be decreased – this could be done by a simple flat insert.

the geometry CU1 is shown to be even much less, $\sigma = 4.62$, and yet the efficiency was found to be low, mere $\eta = 0.348$ as the asymptotic value in the no-spillover state (Fig. 13).

It seemed rather obvious to investigate what improvement, if any, was achievable by making the splitter nose even longer. The tested geometry CU2 with the lengthened splitter resulting in the value σ as small as $\sigma = 3.15$, is presented in Fig. 17. Its properties, as shown in Figs. 18 and 19, were a disappointment, its asymptotic efficiency value only $\eta = 0.203$.

The values of the coefficient Eqs. (12)–(14) were also evaluated and are presented in Fig. 20 in comparison with the original baseline geometry CU1. What the lengthened splitter results in is just an increased relative dissipance q_2 of the first (preferred) collector. Since the general character of the splitter nose shape is similar, it is in this case possible – as shown in Fig. 20 – to guess rather safely the probable properties of the four interpolated cases. Extrapolation is, of course, less safe but on the basis of what is presented in Fig. 20 it may be suggested that a considerable efficiency improvement might be in this case – contrary to common expectations – obtained by choosing the relative distance σ larger. This seems to be an obvious consequence of the dominance of the captive vortex pressure recovery mechanism as discussed in Ref. [13].

7. Rounded splitter nose

A characteristic feature of jet-deflection fluidic devices designed by the present author [6,12,13] is the bi-cuspid nose of the splitter between the two outlet passages. The wall connecting the two cusps is of concave shape. If the jet is deflected by the Coanda effect towards the preferred attachment wall, its outer layer – on the opposite side to the wall – hits one of the cusps, the cusp E shown in Fig. 17. The outer layer is peeled off and turned by following the concave part of the splitter nose, which it leaves in a direction almost opposite to the flow direction of the main part of the deflected jet. The back-turned part flows towards the other, unused attachment wall (the one directed into the vent V) which turns it even more until its trajectory forms nearly a full circle. In the last part of its return trajectory, this backwards flowing fluid is attracted towards the initial part of the main jet due to its entraining, jet-pumping influence. It may also hit upon the main jet by whatever remains from its initial momentum. As a result, the interaction cavity of the valve downstream from the nozzle exit is filled with a standing, captive vortex. This is well visible in the bottom part of Fig. 10. The vortex may entrain some fluid from the vent at $\mu_Y < 1$ or (as in Fig. 10) at $\mu_Y < 1$ may be bleeding some fluid as the spillover flow into V. Nevertheless, over most of the valve operating range (before the switching occurs) it stays there as an

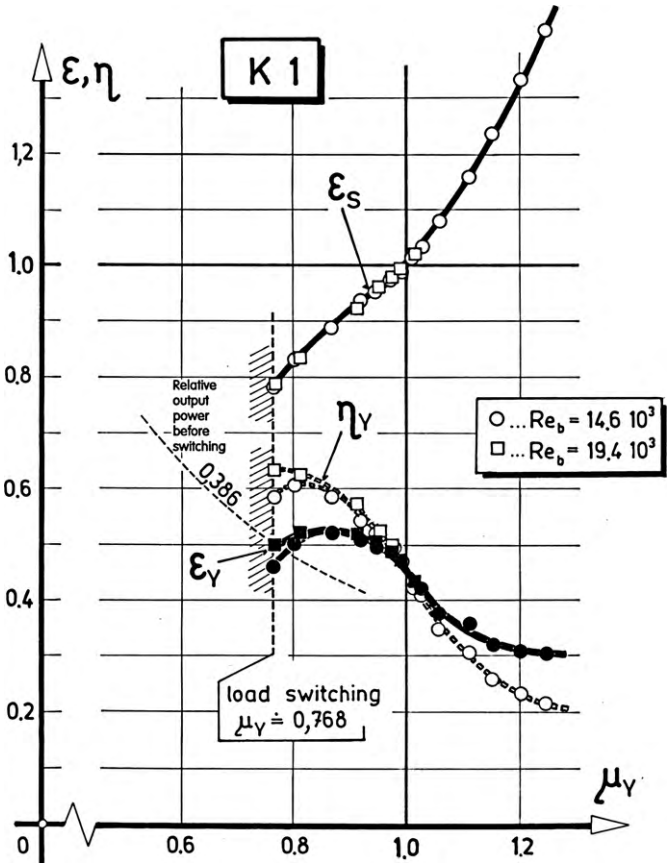

Fig. 28. Experimental complete output characteristic of the valve in the wedge-shaped splitter version K1.

important entity influencing the internal flowfield. In principle, it acts as a positive feedback loop, preventing the jet from separation from the preferential attachment wall. If the jet starts to separate from the attachment wall, its trajectory will be more straight, leading towards the cusp E. The outer layer peeled off by this cusp is more powerful and on its return to the initial part of the jet pushes it more strongly back towards its attachment wall.

Of course, this mechanism extracts more power from the jet than if it were not required to flow past the sharp edge. It may seem to be a reasonable guess that with a smooth, rounded splitter the efficiency would be higher. The opportunity to test this idea was used and an alternative, round-nose splitter geometry RD1 was extemporised as shown in Fig. 21. Without the positive feedback loop, the jet is expected to separate from the attachment wall and load-switch more easily but, after all, the jet attachment in the baseline geometry CU1 is seen in Fig. 12 to be overly stable – the switching there is not a very effective process if it takes place in a situation where already 48.4% of the flow spills over into the vent terminal.

With the rounded splitter RD1, the output characteristic presented in Fig. 22 shows switching indeed occurs at a smaller spillover flow. Comparison of the following Fig. 23 with Fig. 13 shows even some efficiency improvement (44.5% against 34.8%) in the reference state $\mu_Y = 1$, but this is a rather exceptional situation and the overall comparison in Fig. 24 presents a rather unfavourable picture.

The availability of the splitter lengthening component used to set up the geometry CU2 was utilised to investigate the effect of the extremely short nozzle-to-splitter distance $\sigma = 2.59$ in the variant RD2 as presented in Fig. 25. In fact, no good efficiency in this extemporised variant was expected, considering the too small width of the main collector entrance – actually smaller than the nozzle exit width. The result of the measurements in Fig. 26 may be surprising only in finding out that the efficiency decrease relative to Fig. 22 is not very large, mere $\Delta\eta = 4\%$ spread uniformly over the whole of the no-spillover regime. In the jet-pumping regime the difference is larger – obviously due to decreased exposition of the outer side of the jet to the entrainment.

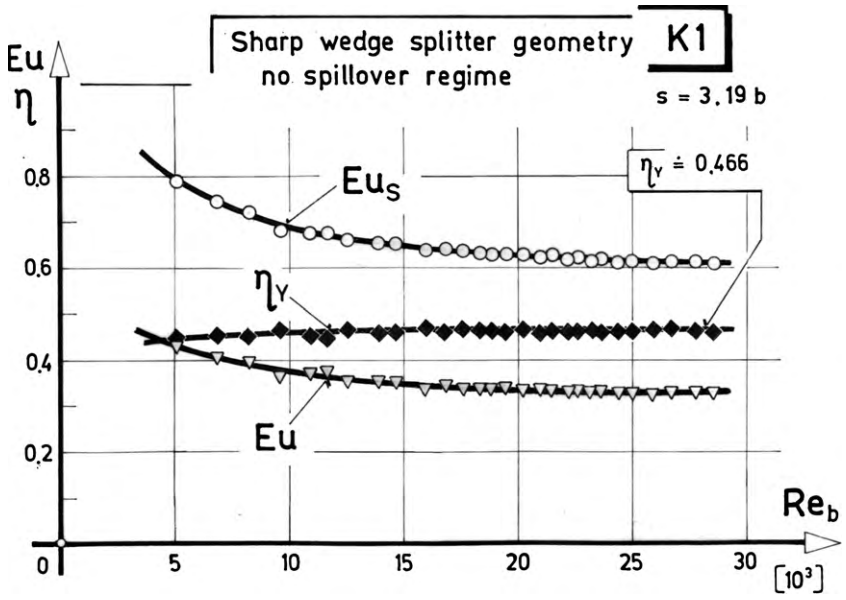

Fig. 29. Euler numbers and efficiency for the variant from Fig. 27.

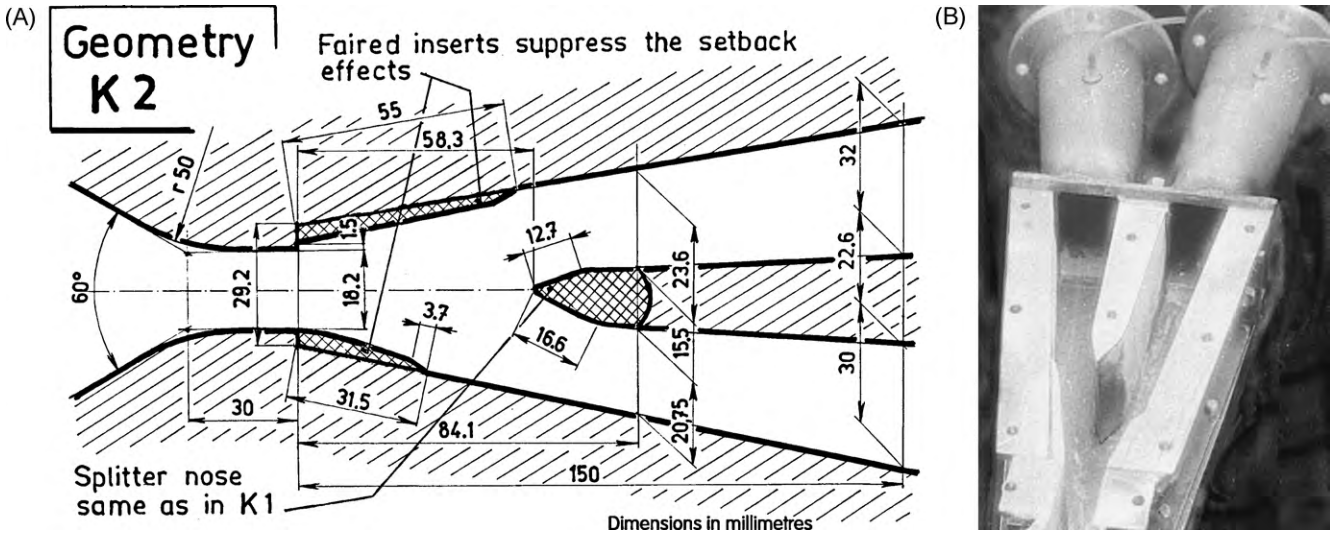

Fig. 30. The significance of the attachment wall setbacks was tested in the valve geometry K2, with the wedge-shaped splitter differing from the case K1 by the setback corners filled on both sides with inserts.

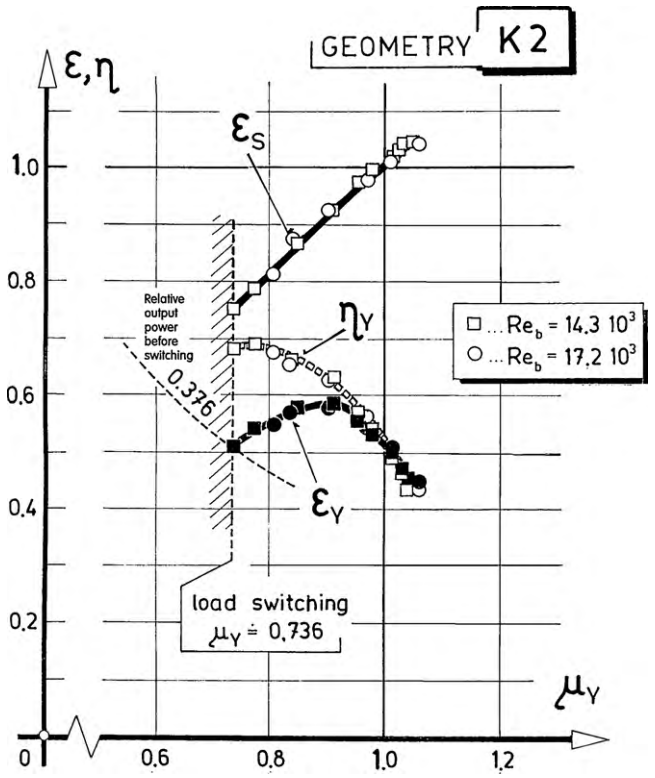

Fig. 31. Output characteristic of the valve in the version K2 shown in Fig. 30. Surprisingly, a comparison with Fig. 28 shows the effect of the setbacks seems to be rather insignificant – just some improvement in efficiency.

8. Wedge-shaped splitter

A question posed quite often is why the splitter in author's valves is not of what seems to be the most obvious shape – simply a wedge with a sharp edge facing the nozzle exit. The present research provided also an opportunity to test this configuration. The small 6.5° apex angle of the splitter walls (Fig. 8) would place the sharp edge designed as their continuation too near to the nozzle; this is why the wedge geometry was tested with a shorter insert facing the exit with the 45° apex (Fig. 27). The lower inclined wall of the insert as shown in Fig. 27 also provided an improved opportunity for the jet entering the preferred collector (leading into Y) with the very small nozzle-to-splitter distance, which in this variant K1 was $\sigma = 3.19$. It has to be admitted that the measurement results, as presented in Fig. 28, are not bad – with the efficiency $\eta = 46.6\%$ they are better than in any of the variants discussed above. The position of the load-switching point is also acceptable. Like in the round (Fig. 23) and other cusp-less variants, the no-spillover efficiency value presented in Fig. 29 is remarkably constant and Reynolds-number independent.

An interesting effect encountered in these experiments was the reluctance – not found in the earlier variants – of the jet to attach at starting the flow to the preferred attachment wall. An improvement in this aspect was achieved by placing at the beginning of this wall, as shown in Fig. 27, a simply shaped (rectangular cross-section) insert, which decreases the effective setback.

Later in version K2, this simple insert was replaced by a more properly shaped one, actually eliminating the setback of the attachment wall completely, as seen in Fig. 30. This, however, produced a too strong attachment, almost eliminating the load-switching effect, which was to be restored by placing a similarly faired insert (with a small setback, however) also on the opposite side. The loading behaviour at the two relatively small Reynolds-number conditions, as presented in Fig. 31, seemed to be quite good. A surprising fact, however, was later revealed by the tests over a wider Re range, presented in Fig. 32: the efficiency was found to decrease almost continuously with increasing Re and near the end of the range fell to a rather poor value.

9. Strange case of Re dependent switching

In one of the performed tests, the inserts filling the setback corners were exchanged, to test the magnitude of their influence. It

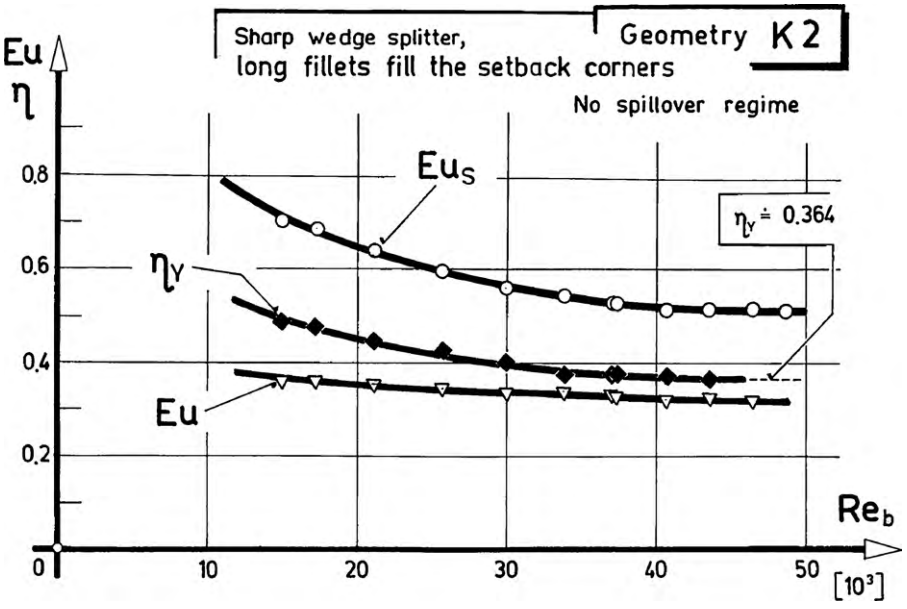

Fig. 32. Euler numbers and efficiency for the value variant from Fig. 30. As could be expected, there is a pronounced Reynolds-number dependence, apparently caused by increased role of wall-friction loss.

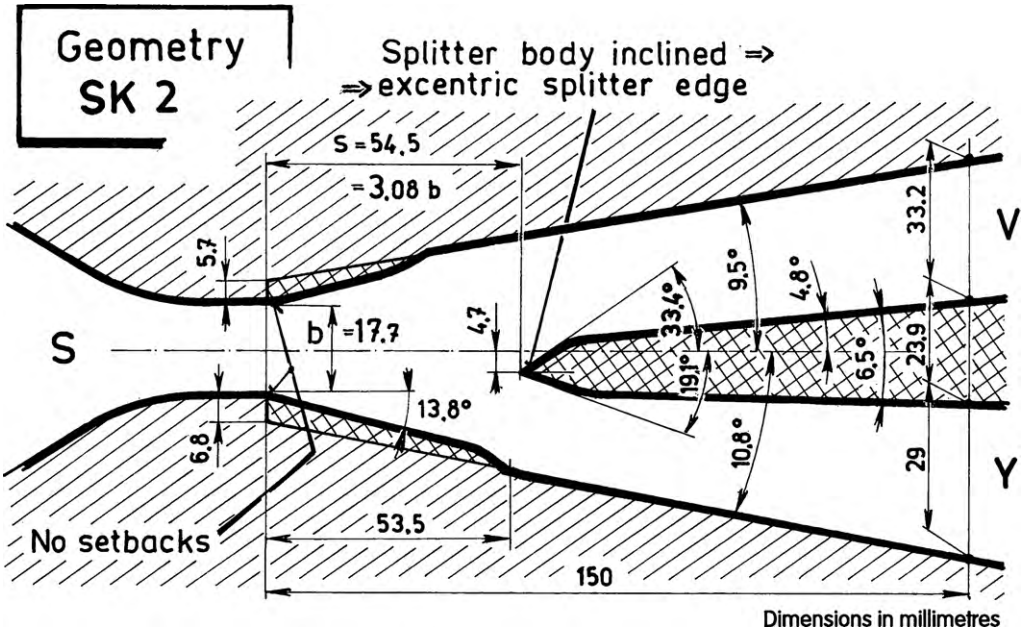

Fig. 33. Valve geometry which demonstrated that the influence of the preferential attachment wall is not as small as could be inferred from comparison of Figs. 28 and 31. Here the preferential wall secures guiding the jet into a significantly narrower main collector entrance.

was discovered that for the proper operation of the valve the splitter had to be placed into the body in an inverted position – with the result, as shown in Fig. 33, of the wedge tip positioned not on the nozzle axis (as was the case in Figs. 27 and 30) but with considerable eccentricity (more than 26% of the nozzle width towards the preferential attachment wall). The completely unexpected behaviour of this SK2 variant was the loss of similarity of loading characteristics: they became so strongly Re-dependent that the data points – as shown in Fig. 34 – failed to fall on a common curve. An even more surprising effect – so far never mentioned in literature – was this Re-dependence continuing so far that at a particular Reynolds number, in the investigated case at $Re = 23.5 \times 10^3$, the available output energy fell to zero (Fig. 35).

No doubt, such behaviour – an automatic change of character when a particular flow rate is reached – may find a number of interesting applications in chemical engineering.

10. Simple supply curves in the output characteristic

Character of the supply curves Eq. (9) as they were found in the output characteristics of the tested valves, may be quite complex, sometimes (e.g., in Figs. 12 and 18) with a sudden change of the behaviour in the no-spillover state $\mu_Y = 1$, while in other cases (e.g., in Figs. 22, 26 and 28) there is no change at all. The specific-energy difference between the supply inlet S and the vent terminal V is obviously mainly dependent on what happens in the interaction cavity of the valve: the loading cannot significantly influence the flow in the nozzle and also whatever changes are there in the vent collector and diffuser are certainly of little influence: the vent in the operating conditions of present interest is practically inactive, with no or very small flow. The large number of accumulated experimental results made possible extensive comparisons, from which it became obvious that a substantial difference in the character of these curves is between the behaviour of convex and concave bi-cuspid splitter shapes. This is obviously due to the different importance of the captive vortex in the interaction cavity [13].

The summary of data for the shapes not promoting this vortex is in Fig. 36. Very surprising – with respect to the typically quadratic or more generally non-linear characteristics of fluid flows – is the fact that Fig. 36 makes obvious: the supply line of the output characteristic in these cases is straight, with positive slope of unity. On the other hand, with most of the splitter shapes having the concave

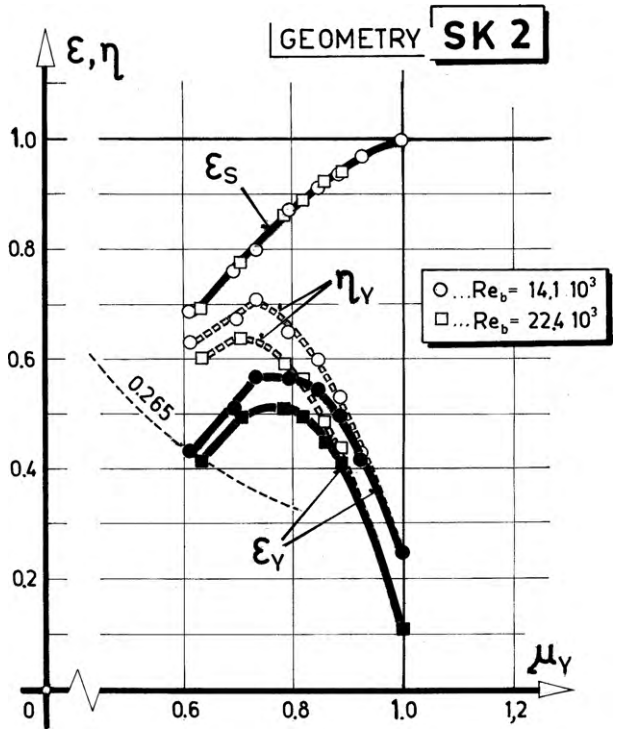

Fig. 34. Output characteristic obtained experimentally with the geometry variant SK2. There is an unusual failure of the characteristics at different Reynolds number to form a single universal line in the similarity co-ordinates.

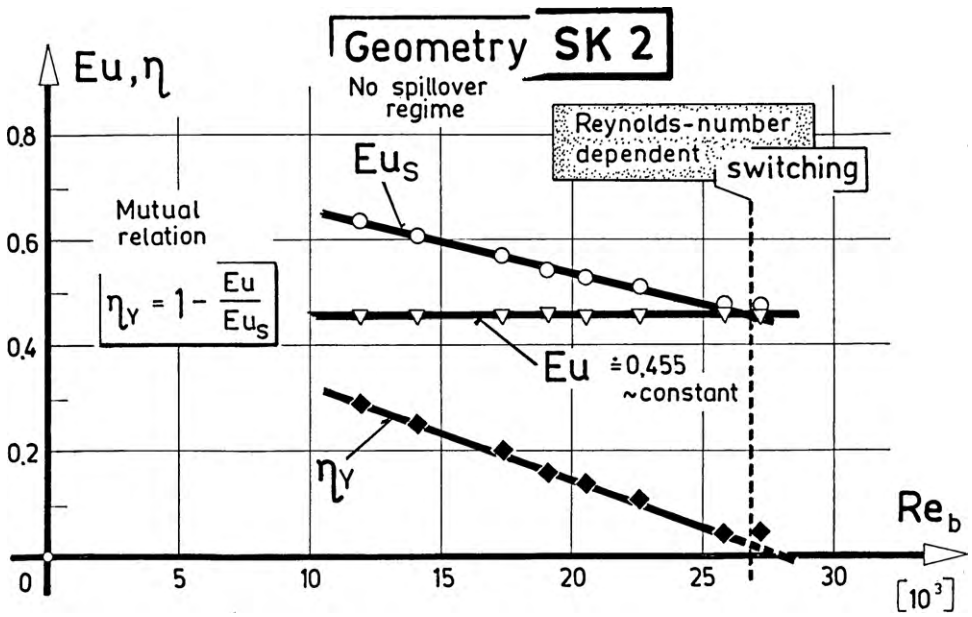

Fig. 35. Euler numbers and efficiency dependence on Reynolds number for the valve variant from Fig. 33 explains the failure of the similarity transformation in the previous Fig. 34. Very special property found in this variant is the existence of the limiting flow rate at which the Coanda effect fails to keep the jet attached in a situation different from the load-switching.

wall between the two cusps, the supply line (Fig. 37) is also linear with negative slope magnitude −1.0. Within these shapes there are more exceptional cases, one of them (actually the baseline case CU1) exhibiting slope magnitude −0.5.

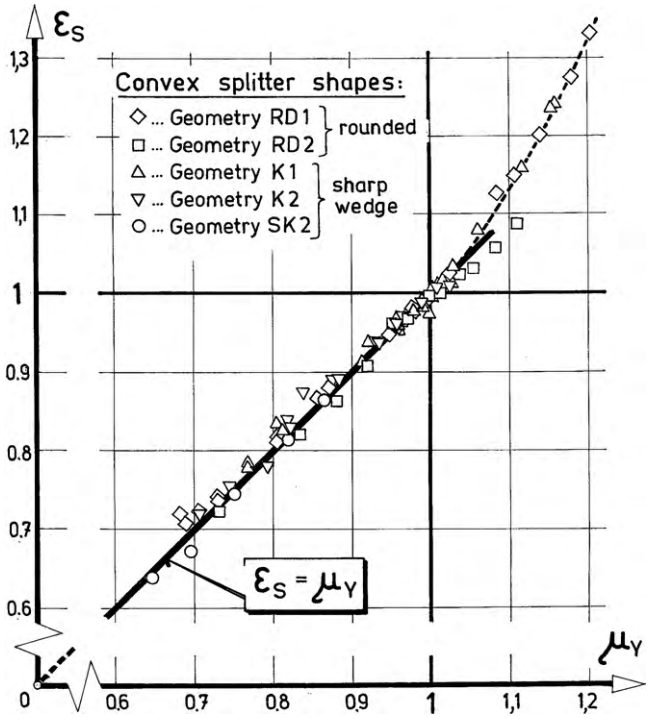

Fig. 36. Measurements of the changes in the supply specific-energy drop with loading of the valve has shown a remarkable identity of the dependence for all geometries without the internal feedback: in the similarity co-ordinates the dependence is a simple linear proportionality.

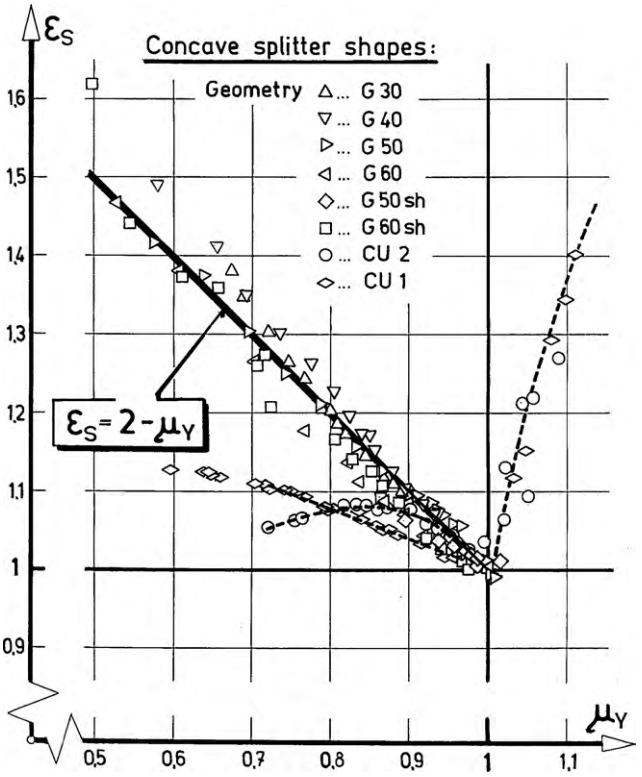

Fig. 37. Similar plotting of the experimental results as in Fig. 36 for all investigated geometry variants with the bi-cuspid splitter noses generating the internal feedback.

11. Conclusions

Performed extensive experimental investigations of various alternative designs of a no-moving-part valve switching the flow into a different outlet, when experiencing a certain critical level of output loading, demonstrate that this is a device that deserves

being better known in chemical engineering circles. The absence of any control circuits and of other sensitive and delicate instrumentation means such a valve may be easily – and inexpensively – made form materials making the valve resistant to extreme operating conditions (high temperature, vibration, or nuclear radiation) and capable of directing the flows of difficult to handle fluids – such as, e.g., hot gas, molten metals, or chemically aggressive liquids. The accumulated data provide useful information to designing such valves. The paper brings to attention several interesting new aspects, such as the characterisation by the third-order tensor, strange Re-dependent switching, and the linear +1 or −1 slope loading dependence of the supply energy difference in the similarity-transformed co-ordinates.

Acknowledgements

The author gratefully acknowledges the financial support by research grant IAA200760705 and by the research plan AV0Z20760514 provided by the Grant Agency of the Academy of Sciences of the Czech Republic – as well as by the grant 101/07/1499 from the Grant Agency of the Czech Republic.

References

[1] V. Tesař, Extremely simple pressure regulator—computation studies, Chemical Engineering Journal 155 (2009) 361.
[2] T. Scanlon, P. Wilson, G. Priestman, J. Tippetts, Development of a novel flow control device for limiting the efflux of air through a failed pipe, in: Proceedings of ASME Turbo Expo 2009, Paper GT2009, Orlando, Florida, USA, 2009.
[3] V. Tesař, Fluidic control of molten metal flow, Acta Polytechnica: Journal of Advanced Engineering 43 (1) (2003) 15, ISSN 1210-2709.
[4] V. Tesař, Fluidic valve for reactor regeneration flow switching, Chemical Engineering Research and Design, Part A 82 (A3) (2004) 1.
[5] V. Tesař, Fluidic valves for variable-configuration gas treatment, Chemical Engineering Research and Design, Part A 83 (September (A9)) (2005) 1111–1121.
[6] V. Tesař, Fluidic control of reactor flow—pressure drop matching, Chemical Engineering Research and Design 87 (6) (2009) 817.
[7] V. Tesař, et al., New ways of fluid flow control in automobiles: experience with exhaust gas after treatment control, in: Proceedings of World Automobile Congress, Paper No. F2000H192, Society of Automotive Engineers, Seoul, Korea, June 2000, p. 167, ISBN 89-85000-00-4 98550.
[8] V. Tesař, Law for pressure loss in monolithic reactor matrices, in: Proceedings of Colloquium "Fluid Dynamics'98", Institute of Thermomechanics, Academy of Sciences of the Czech Republic, Prague, October 1998, p. 49, ISBN 80-85918-45-5.
[9] J.R. Tippetts, J.K. Royle, Design of flow control circuits involving bistable fluid amplifiers, Fluidics Quarterly 3 (4) (1971) 1.
[10] J.R. Tippetts, Development Needs, NATO agency for aeronautical research and development AGARDograph 215 (1976).
[11] N.K. Ibragimov, Elementary Lie Group Analysis and Ordinary Differential Equations, Wiley, New York, 1999.
[12] V. Tesař, C.-H. Hung, W. Zimmerman, No-moving-part hybrid-synthetic jet actuator, Sensors and Actuators A 125 (2) (2006) 159.
[13] V. Tesař, Mechanism of pressure recovery in jet-type actuators, Sensors and Actuators A: Physical 152 (2009) 182–191.
[14] V. Tesař, Pressure-driven Microfluidics, Artech House, Boston, USA, 2007.
[15] Fluidic circuits, in: W.B.J. Zimmerman (Ed.), Microfluidics: History, Theory, and Applications, Springer-Verlag, Wien/New York, 2006, pp. 255–304, CISM Courses and Lectures No. 466, ISBN-10-3-211-32994-3.
[16] L.N. Trefethen, A.E. Trefethen, S.C. Reddy, T.A. Driscoll, Hydrodynamic stability without eigenvalues, Science 261 (5121) (1993) 578.
[17] V. Tesař, W.B.J. Zimmerman, G. Regunath, Helical instability structures in swirling jets, Proceedings of the 8th Internat. Symp. on Fluid Control. Measurement, and Visualization FLUCOME 2005, Chengdu, China (2005).
[18] V. Tesař, Characterisation of three-terminal fluidic elements and solution of bifurcated-flow circuits using the concept of equivalent dissipance, Journal of Fluid Control/Fluidics Quarterly 13 (1981) 55.